BMC Cancer

RESEARCH Open Access

RPS6KA1 is a histone acetylation-related oncoprotein in acute myeloid leukemia which is targeted by afzelin

Xiaojuan Guo[1†], Guinian Huang[1†], Dafa Qiu[1], Huiqing He[1], Xiaomin Niu[1], Ziwen Guo[1*] and Yongbin Ye[1*]

Abstract

Background Histone acetylation plays a critical role in the progression of acute myeloid leukemia (AML). This study aimed to explore the prognostic significance and biological implications of histone acetylation-related genes in AML and to identify potential oncoproteins and therapeutic compounds.

Methods Genes associated with AML and histone acetylation were identified using the TCGA-LAML and IMEx Interactome databases. A histone acetylation-related risk model was developed using the least absolute shrinkage and selection operator method. The prognostic value of the model was evaluated through Kaplan-Meier survival analysis, time-dependent receiver operating characteristic curve, univariate and multivariate Cox regression, and nomogram calibration. Key genes were identified using random forest, support vector machine, and multivariate Cox analysis. Molecular docking was employed to assess the binding affinity between ribosomal protein S6 kinase A1 (RPS6KA1) and potential compounds. Furthermore, the effects of RPS6KA1 and afzelin on the malignant behaviors and downstream pathways of AML cells were validated through in vitro experiments.

Results A risk model composed of 6 genes, including *HDAC6*, *CREB3*, *KLF13*, *GOLGA2*, *RPS6KA1* and *ZMIZ2*, was established, demonstrating strong prognostic predictive capability. Among these, RPS6KA1 emerged as a key risk factor linked to histone acetylation status in AML. Elevated RPS6KA1 expression was observed in AML samples and was associated with poor prognosis. RPS6KA1 knockdown suppressed AML cell proliferation, migration, and invasion, induced G0/G1 phase arrest, and promoted apoptosis. Additionally, RPS6KA1 was identified as a potential target for afzelin, which exhibited anti-AML activity by inactivating RPS6KA1.

Conclusion Histone acetylation status is closely associated with AML patient prognosis. RPS6KA1 acts as an oncoprotein in AML, facilitating disease progression. Afzelin may represent a novel therapeutic agent for AML by targeting RPS6KA1, which requires validation by clinical trials.

Keywords Acute myeloid leukemia, Histone acetylation, RPS6KA1, Prognosis, afzelin

†Xiaojuan Guo and Guinian Huang contributed equally.

*Correspondence:
Ziwen Guo
zsgzw@21cn.com
Yongbin Ye
zsyongbiny1984@163.com
[1]Department of Hematology, Zhongshan People's Hospital, Zhongshan 528403, Guangdong, China

Introduction

Acute myeloid leukemia (AML) is a highly lethal malignancy originating from myeloid stem/progenitor cells [1, 2]. It is the most common form of acute leukemia in adults, accounting for approximately 80% of all diagnosed cases [3]. The incidence of AML increases with age, and in 2021, around 20,240 new cases and 11,400 deaths were reported globally [4]. Despite chemotherapy with cytarabine and anthracyclines remaining the standard treatment for AML [5], the 5-year overall survival (OS) rate is only approximately 40% for patients under 60 years of age, while it drops to just 10% for those over 60 [6, 7]. These statistics underscore the urgent need for a deeper understanding of the mechanisms driving AML progression and the development of novel therapeutic strategies.

Epigenetic modifications regulate gene expression through various mechanisms, including histone modification, DNA methylation, non-coding RNA regulation, and chromatin structure remodeling [8]. In eukaryotic cells, histone modifications, such as acetylation, phosphorylation, methylation, sumoylation, and ubiquitination, contribute significantly to molecular functional diversity [9]. Histone acetylation, a reversible process mediated by histone acetyltransferases (HATs) and histone deacetylases (HDACs), alters chromatin structure and gene expression [10, 11]. Aberrant histone acetylation has been implicated in the pathogenesis of various cancers, such as breast, colon, lung, liver, pancreatic, prostate, thyroid carcinomas, and AML [12–14]. Targeting these epigenetic alterations holds great promise for cancer therapy [15–18]. Understanding the clinical significance of dysregulated histone acetylation can aid in the development of new therapeutic strategies for AML.

In this study, we developed a robust and sensitive prognostic risk model based on histone acetylation regulators. Notably, ribosomal protein S6 kinase A1 (*RPS6KA1*), identified as a key risk factor in this model, was found to be highly expressed in AML patients and to promote malignant behaviors in AML cell lines. Furthermore, we discovered that afzelin has a high binding affinity for RPS6KA1 and exhibits tumor-suppressive effects in AML cell lines.

Methods and materials

Data collection

RNA sequencing data, clinicopathological characteristics, and gene mutation information for 132 AML samples were obtained from The Cancer Genome Atlas (TCGA) database. RNA-seq transcriptome data were converted into fragments per kilobase of exon model per million mapped fragments (FPKM) format and subsequently normalized using the SVA package. Additionally, the GSE71014 dataset was downloaded from the Gene Expression Omnibus (GEO) database (https://www.ncbi.nlm.nih.gov/geo/) to serve as a validation set.

Identification of genes associated with histone acetylation

A total of 36 histone acetylation regulators were identified through a comprehensive literature review. To identify genes associated with histone acetylation, Pearson correlation analysis was performed based on gene expression data from the TCGA-LAML cohort. The selection criteria were a correlation coefficient > 0.7 and $P < 0.05$. Additionally, genes interacting with these 36 histone acetylation regulators were identified using the IMEx Interactome database (http://www.innatedb.com). By combining the genes identified through these methods, a gene-gene interaction network was constructed, and the hub genes were identified and designated as "histone acetylation-related genes."

Construction and validation of histone acetylation-related risk model

The TCGA-LAML dataset was randomly divided into a training set and a test set in a 7:3 ratio. In the training set, least absolute shrinkage and selection operator (LASSO)-Cox regression analysis was employed to identify key genes for constructing the risk model. The risk score for each patient was calculated using the following formula: risk score = ∑ (coefficient × expression of signature gene). The final risk score was calculated as follows: ultimate risk score = $-0.0020 \times HDAC6 + 0.0053 \times CREB3 + 0.0013 \times KLF13 - 0.0461 \times GOLGA2 + 0.0091 \times RPS6KA1 - 0.0022 \times ZMIZ2$. Patients in the training cohort ($n=93$), test cohort ($n=39$), TCGA-LAML cohort ($n=132$), and GSE71014 cohort ($n=104$) were stratified into low-risk and high-risk groups based on the median risk score. Kaplan-Meier survival analysis and the log-rank test were performed to compare the prognosis of patients in the high- and low-risk groups. The sensitivity and specificity of the risk model were evaluated using time-dependent receiver operating characteristic (ROC) curves and the corresponding area under the curve (AUC) values. Principal component analysis (PCA) was conducted using the ggplot2 package in R. Univariate and multivariate Cox regression analyses were employed to assess the impact of risk scores and clinicopathological factors (age, sex, and tumor type) on prognosis, with hazard ratios (HR) calculated for each factor.

Construction and verification of nomogram

A nomogram was constructed based on the TCGA-LAML cohort by integrating clinicopathological variables such as age, gender, tumor type, and risk scores. This was done using the "nomogram" package in R software to further explore the individual prognosis of AML patients.

Calibration and ROC curve analyses were conducted to assess the predictive performance of the nomogram from various perspectives.

Identification and enrichment analysis of differentially expressed genes (DEGs) in risk groups

DEGs between the high-risk and low-risk groups in the TCGA-LAML dataset were identified using the R software package DESeq2, with the screening criteria set at |log fold change| > 1 and $P<0.05$. Subsequently, the Kyoto Encyclopedia of Genes and Genomes (KEGG) pathway analysis of DEGs was performed using the clusterProfiler package in R.

Immune cell infiltration and genome mutation analysis

The CIBERSORT method was employed to evaluate differences in immune cell infiltration between the different groups. Immune infiltration, including immune, stromal, and ESTIMATE scores, was assessed using the Estimation of Stromal and Immune Cells in Malignant Tumors using Expression Data (ESTIMATE) algorithm. The correlation between immune infiltration, risk scores, and RPS6KA1 expression was analyzed. Waterfall plots were generated using the maftools package in R to visualize the genomic mutation landscape.

Network construction and analysis of RPS6KA1 and its co-expressed genes

The interaction network of *RPS6KA1* and its co-expressed genes was constructed using GeneMANIA (http://genemania.org/). Additionally, gene ontology (GO) and KEGG analyses were performed using the clusterProfiler package in R. The expression level of *RPS6KA1* and the survival status of AML patients were analyzed using the GEPIA database (http://gepia.cancer-pku.cn/).

Molecular docking

Potential compounds that bind to RPS6KA1 were identified from the HERB database (http://herb.ac.cn/). The X-ray crystal structure of the RPS6KA1 protein was obtained from the Protein Data Bank (PDB; https://www.rcsb.org/). The PDB file was processed with PyMOL software. The 3D chemical structures of potential compounds were downloaded from PubChem (https://www.ncbi.nlm.nih.gov/pccompound/) in SDF format, then converted to PDB format using OpenBabel 3.1.1. Subsequently, the PDB files were converted to PDBQT format using AutoDockTools (version 1.5.7). AutoDock Vina v.1.1.2 was used for blind docking to calculate the binding energy, with the receptor grid encompassing the entire protein and docking performed at an exhaustiveness level of 2000. The structure with the lowest binding free energy was selected as the most favorable, with a binding energy < 0 indicating that the ligand can spontaneously bind to the receptor [19]. The docking results were visualized using PyMOL software.

Cell culture, transfection, and treatment

Human AML cell lines HL-60 and THP-1 (ATCC, Manassas, VA, USA) were cultured in Dulbecco's Modified Eagle's Medium (DMEM; Invitrogen, Carlsbad, CA, USA) supplemented with 10% fetal bovine serum (FBS; Invitrogen, Carlsbad, CA, USA), 100 U/mL penicillin, and 100 μg/mL streptomycin (Invitrogen, Carlsbad, CA, USA). Cells were maintained in a humidified incubator at 37 °C with 5% CO_2. When cells reached 70–80% confluence, Lipofectamine 2000 (Invitrogen, Carlsbad, CA, USA) was used for transfection. Small interfering RNA (siRNA) targeting *RPS6KA1* (si-RPS6KA1) (GenePharma Co., Ltd., Shanghai, China) and corresponding negative controls (si-NC) were transfected into HL-60 and THP-1 cells. The transfection efficiency was assessed 24 h post-transfection using quantitative real-time PCR (qPCR). Additionally, HL-60 and THP-1 cells were treated with afzelin (purity: 99.62%, CAS No. HY-N1441; MedChemExpress, Shanghai, China) at varying concentrations (0, 10, 20, 30, 40, and 50 μM) for 24 h. Untreated cells served as controls.

qPCR

Total RNA from HL-60 and THP-1 cells was extracted using the TRIzol kit (Takara, Dalian, China). Complementary DNA was synthesized with the Transcriptor Universal cDNA Master kit (Roche, Shanghai, China). Real-time PCR was conducted using a SYBR Green PCR Master Mix Kit (LMAI Bio, Shanghai, China) on an ABI7500 real-time PCR system (Applied Biosystems, San Francisco, CA, USA). *GAPDH* was used as an internal reference. The primer sequences are as follows: *RPS6KA1*: 5'-ATGCAGACCCCAGCAGATTT-3' (forward) and 5'-GTGCAGCTTCACCACGAATG-3' (reverse); *GAPDH*: 5'-GAAGGTGAAGGTCGGAGTC-3' (forward) and 5'-GAAGATGGTGATGGGATTCGATTC-3' (reverse).

Cell counting kit-8 (CCK-8) assay

HL-60 and THP-1 cells were seeded in 96-well plates at a density of 1,000 cells per well in 100 μL of medium and cultured at 37 °C with 5% CO_2 for 24 h. At specific time points (0, 1, 2, 3, and 4 days), 10 μL of CCK-8 solution (Dojindo, Kumamoto, Japan) was added to each well. After a 2-hour incubation, the absorbance of each well was measured at a wavelength of 450 nm using a microplate reader (Bio-Rad, Richmond, CA, USA). Cell viability was calculated using the following formula: Cell viability (%) = (OD treatment-OD blank)/(OD control-OD blank) × 100%.

Transwell assays

Transwell chambers with 8 μM pore size (Costar, Cambridge, MA, USA) were used to assess cell migration and invasion. For the invasion assay, chambers were coated with Matrigel (BD Biosciences, Franklin Lakes, NJ, USA); Matrigel was not used for the migration assay. HL-60 and THP-1 cells (approximately 5×10^4 cells) were suspended in 200 μL of serum-free medium and added to the upper chamber. The lower chamber was filled with 600 μL of medium containing 10% FBS. Cells were then incubated at 37 °C with 5% CO_2 for 24 h. The number of cells that migrated or invaded to the lower chamber was then counted using a hemocytometer.

Flow cytometry

As previously described [20], the cell cycle and apoptosis of AML cell lines were analyzed using flow cytometry. For the cell cycle assay, HL-60 and THP-1 cells were collected and centrifuged at room temperature (800×g) for 10 min. The cells were then incubated with cold 70% ethanol for 24 h, followed by staining in the dark with propidium iodide (PI)/RNase stain buffer (BD Pharmingen, San Diego, CA, USA) for 15 min. DNA content was analyzed using the Guava Easycyte HT flow cytometer system (Merck KGaA, Darmstadt, Germany), and the results were processed using ModFit 3.2 software (Verity Software House, Topsham, ME, USA). For apoptosis detection, AML cells were stained with 10 μL of Annexin V-Fluorescein Isothiocyanate (FITC) and 10 μL of PI in the dark at room temperature for 15 min. The cells were then sorted by flow cytometry. The percentages of Annexin V–/PI+ (necrosis), Annexin V+/PI– (early apoptosis), and Annexin V+/PI+ (late apoptosis) cells were calculated.

Western blotting

AML cells were lysed using RIPA lysis buffer containing protease inhibitors (Sigma, St. Louis, MO, USA) to extract total cellular protein. Protein concentration was quantified using a BCA kit (Beyotime, Shanghai, China). After separation by sodium dodecyl sulfate-polyacrylamide gel electrophoresis, the proteins were transferred onto a polyvinylidene fluoride (PVDF) membrane (Millipore, Billerica, MA, USA). The membrane was then blocked with 5% skim milk at room temperature for 2 h. Subsequently, the PVDF membrane was incubated overnight at 4 °C with the following primary antibodies: anti-RPS6KA1 (ab32114, 1:1000, Abcam), anti-phospho (p)-RPS6KA1 (T359) (ab32413, 1:1000, Abcam), anti-ERK1/2 (ab184699, 1:1000, Abcam), anti-p-ERK1/2 (T202/Y204) (ab278538, 1:1000, Abcam), anti-p-JNK (T183/Y185) (ab307802, 1:1000, Abcam), anti-JNK (ab179461, 1:1000, Abcam), anti-p-p38 (T180) (ab178867, 1:1000, Abcam), anti-p38 (ab170099, 1:1000, Abcam), anti-p-MCL-1 (bs-18726R, Bioss, Beijing, China), and anti-GAPDH (ab9485, 1:1000, Abcam). The membrane was then incubated with goat anti-rabbit IgG H&L (HRP) secondary antibody (ab205718, 1:5000, Abcam) at room temperature for 1 h. Protein bands were visualized using the BeyoECL Plus kit (Beyotime, Shanghai, China). Densitometric analysis of the bands was performed using ImageLab software version 4.1 (Bio-Rad Laboratories, Hercules, CA, USA).

Statistical analysis

GraphPad Prism 8.0 (GraphPad Software Inc., San Diego, CA, USA) and SPSS 21.0 software (IBM Corp., Armonk, NY, USA) were used for statistical analysis. For in vitro assays, data are presented as the mean ± standard deviation (SD). All experiments were performed independently in triplicate. Comparisons between groups were made using Student's t-test or one-way analysis of variance with Tukey's post hoc test. A P-value < 0.05 was considered statistically significant.

Results

Construction and analysis of histone acetylation-related gene risk model in AML

A total of 36 histone acetylation regulatory genes were identified (Supplementary Table 1). Pearson correlation analysis revealed 1,988 genes in the TCGA-LAML dataset that were associated with these 36 histone acetylation regulators. Additionally, 2,035 genes associated with these regulators were identified in the IMEx Interactome database. The interrelationships among all these genes were combined to construct a gene interaction network (Fig. 1A), from which 301 key genes were identified and termed histone acetylation-related genes. LASSO-Cox regression analysis with ten-fold cross-validation was then performed on TCGA-LAML training cohort to determine the optimal tuning parameter λ (Fig. 1B). Six genes, including *HDAC6*, *CREB3*, *KLF13*, *GOLGA2*, *RPS6KA1*, and *ZMIZ2*, were selected based on the optimal λ value (0.14) to construct the risk model (Fig. 1C). AML patients in the TCGA-LAML cohort (n=132), training cohort (n=93), test cohort (n=39), and GSE71014 cohort (n=104) were stratified into high-risk and low-risk groups using the median risk score as the threshold. The patients in the high-risk group had significantly shorter overall survival in all four cohorts compared to those in the low-risk group (Fig. 1D-G). Additionally, ROC curve analysis was used to assess the accuracy and sensitivity of the risk model. The model demonstrated strong predictive value for evaluating the prognosis of patients in both the TCGA-LAML and GSE71014 cohorts. The 1-year, 3-year, and 5-year AUC values for the TCGA-LAML cohort were 0.70, 0.79, and 0.95, respectively (Fig. 1H). For the GSE71014 cohort, the

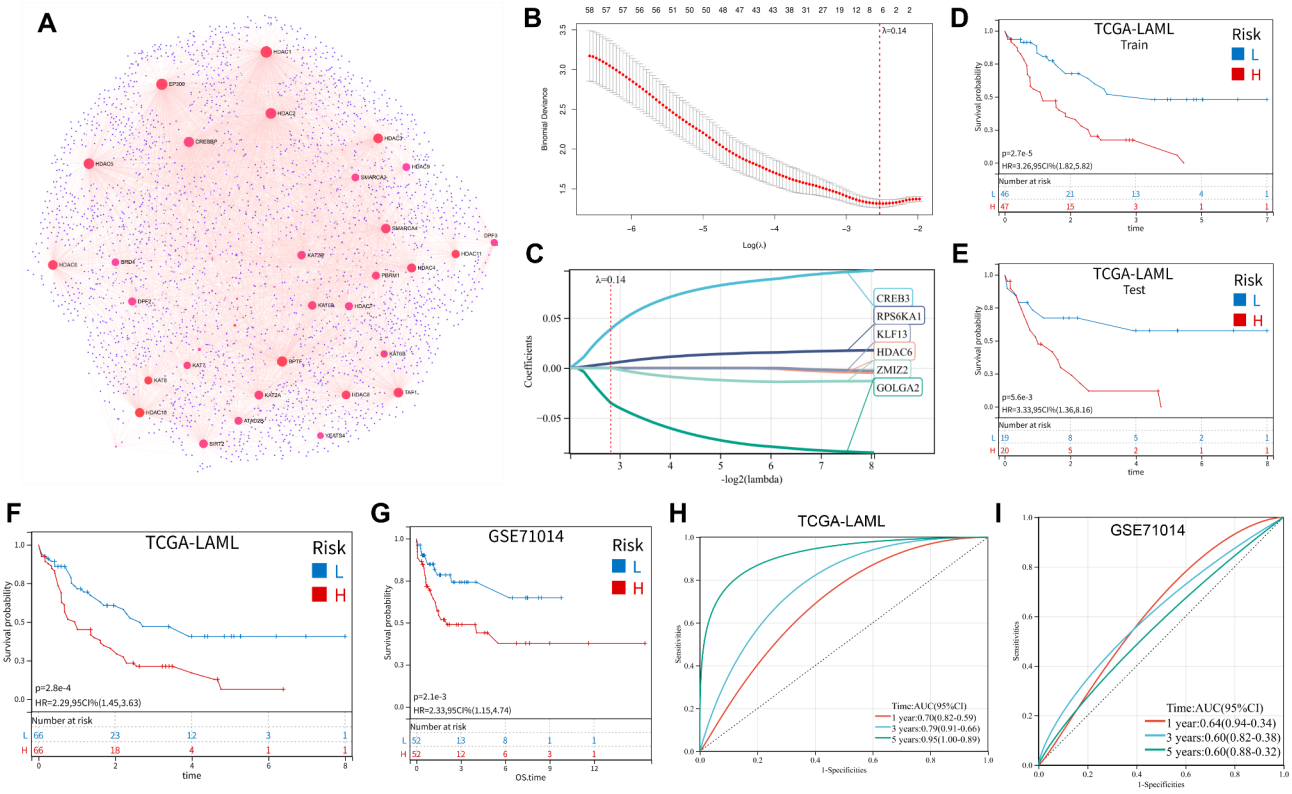

Fig. 1 Construction and verification of risk model. **A**. Gene-gene interaction network based on 36 histone acetylation regulators. **B**. 10-fold cross-validation in the LASSO analysis. **C**. LASSO coefficient profiles of histone acetylation-related genes in the TCGA-LAML dataset, from which six genes were selected to construct the risk model. D-G. Overall survival of high-risk and low-risk patients in the TCGA-LAML training cohort **(D)**, test cohort **(E)**, general cohort **(F)**, and GSE71014 cohort **(G)** was analyzed by Kaplan-Meier analysis. H-I. Time-dependent ROC analysis of risk scores in TCGA-LAML cohort and GSE71014 cohort

1-year, 3-year, and 5-year AUC values were 0.64, 0.60, and 0.60, respectively (Fig. 1I). Overall, these findings suggest that the risk model has strong predictive power for AML patient prognosis, implying that abnormal histone acetylation is closely associated with AML progression.

Construction and evaluation of nomogram

PCA revealed distinct gene expression patterns between patients in different risk groups within the TCGA-LAML cohort (Supplementary Fig. 1A), indicating that the model effectively distinguishes high-risk patients from low-risk patients. Additionally, in the TCGA-LAML cohort, *CREB3*, *KLF13*, and *RPS6KA1* were highly expressed in the high-risk group, while *ZMIZ2*, *HDAC6*, and *GOLGA2* were expressed at lower levels in the high-risk group (Supplementary Fig. 1B). Univariate and multivariate Cox regression analyses were performed on the TCGA-LAML cohort, incorporating risk scores and clinical variables. The results (Supplementary Fig. 1C&D) demonstrated that, aside from gender, risk score, tumor type (M0-M7), and age could serve as independent prognostic factors for AML patients. A nomogram was constructed to predict 1-, 3-, and 5-year survival probabilities for AML patients (Supplementary Fig. 1E). Calibration curves showed that the predicted 1-, 3-, and 5-year overall survival closely matched the observed overall survival times (Supplementary Fig. 1F). ROC curve analysis indicated that in the TCGA-LAML cohort, the AUC values for the 1-, 3-, and 5-year nomogram were 0.70, 0.75, and 0.84, respectively (Supplementary Fig. 1G). These findings suggest that the nomogram has strong clinical utility in predicting the prognosis of AML patients.

Gene enrichment and immunoinfiltration analysis

To explore the pathways associated with the risk score, differential gene expression analysis was performed between the low- and high-risk groups. The analysis identified 1,390 DEGs, with 496 up-regulated and 894 down-regulated in the high-risk group compared to the low-risk group (Fig. 2A; Supplementary Table 2). KEGG pathway enrichment analysis revealed that the 894 down-regulated genes were associated with transcriptional dysregulation in cancer and acute myeloid leukemia (Fig. 2B). The 496 up-regulated genes were primarily enriched in pathways such as cytokine-cytokine receptor interaction, osteoclast differentiation, chemokine signaling pathway,

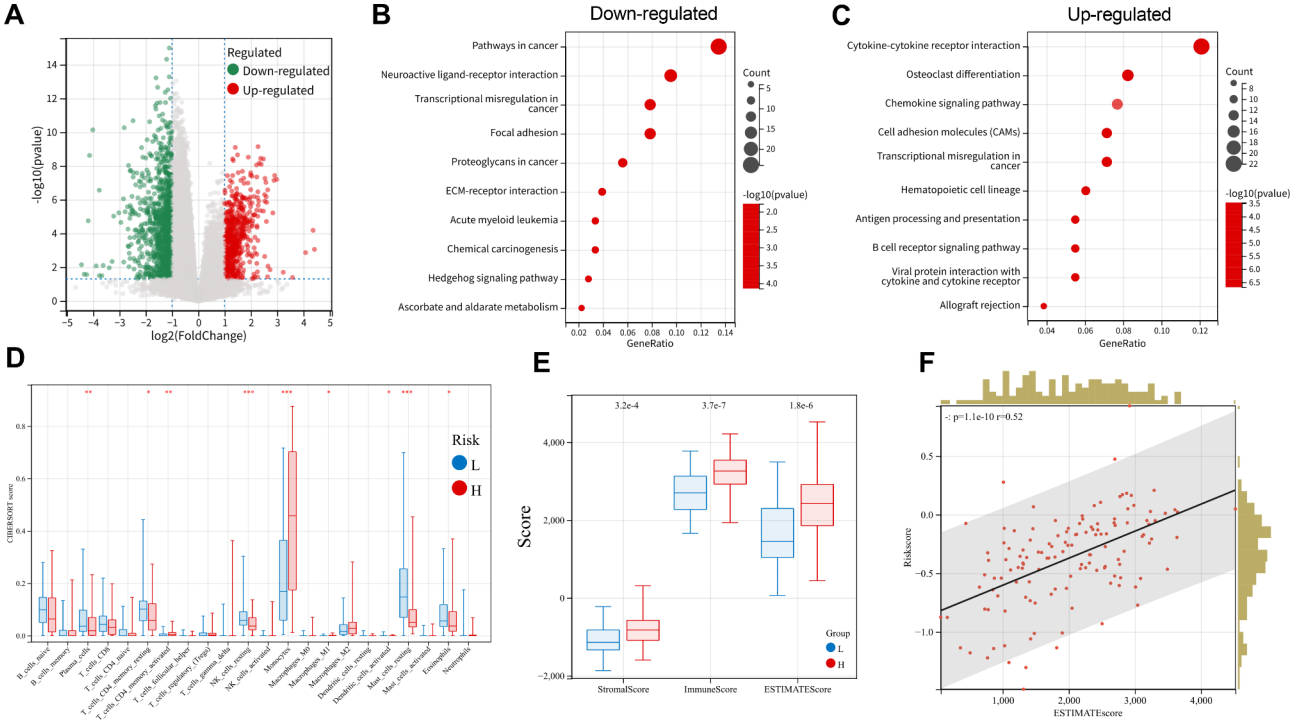

Fig. 2 Analysis of functional enrichment and immune infiltration. **A**. Volcano plot showing DEGs between low- and high-risk groups in the TCGA-LAML dataset. A total of 496 genes were up-regulated (red dots) and 894 genes were down-regulated (green dots). The screening criteria were $P < 0.05$ and $\log_2|\text{fold change}| > 1$. B&C. Enrichment results of KEGG pathway of lowly-expressed genes **(B)** and highly expressed genes **(C)**. The horizontal axis represents the gene ratio, and the color and size of the bubble represent the *p*-value and the gene count, respectively. **D**. Immune infiltration differences between high- and low-risk groups were evaluated using the CIBERSORT method. **E**. Immune infiltration differences between high- and low-risk groups were evaluated using the ESTIMATE method. **F**. Relationship between risk score and immune infiltration score

cell adhesion molecules (CAMs), and transcriptional misregulation in cancer (Fig. 2C). Additionally, the relationship between the tumor microenvironment and risk scores was analyzed. The CIBERSORT algorithm indicated significant differences in immune cell infiltration between the two groups ($P<0.05$, Fig. 2D). The ESTIMATE algorithm showed that stromal, immune, and ESTIMATE scores were significantly higher in high-risk patients compared to low-risk patients ($P<0.05$, Fig. 2E). Correlation analysis further demonstrated a positive correlation between the risk score and immune infiltration score (Fig. 2F).

Screening of key prognostic genes in AML

Multivariate Cox regression analysis of the six genes included in the risk model identified *GOLGA2* as an independent protective factor, while *CREB3* and *RPS6KA1* emerged as independent risk factors affecting the prognosis of AML patients (Fig. 3A). To further identify key genes associated with AML prognosis, random forest and support vector machine methods were employed. The results indicated that *RPS6KA1* was the most significant prognostic risk gene (Fig. 3B&C). Subsequently, the relationship between *RPS6KA1* expression and AML immune infiltration was analyzed, revealing a significant positive correlation between the two (Fig. 3D). Additionally, TCGA-LAML samples were stratified into high and low expression groups based on *RPS6KA1* expression levels. The mutation landscape analysis showed that the high *RPS6KA1* expression group had a higher frequency of AML-related gene mutations (Fig. 3E). ROC curve analysis demonstrated that the expression level of the *RPS6KA1* gene could effectively predict the prognosis of AML patients (Fig. 3F).

Enrichment analysis of RPS6KA1 and its co-expressed genes

Based on the GeneMania database, the interaction network of *RPS6KA1* and its co-expressed genes was constructed. Notably, *RPS6KA1* and its co-expressed genes were found to be involved in the regulation of histone deacetylation (Fig. 4A). Further GO and KEGG enrichment analyses revealed that these genes were primarily associated with the positive regulation of growth (Fig. 4B). Additionally, they were enriched in multiple pathways including MAPK signaling pathway (Fig. 4C).

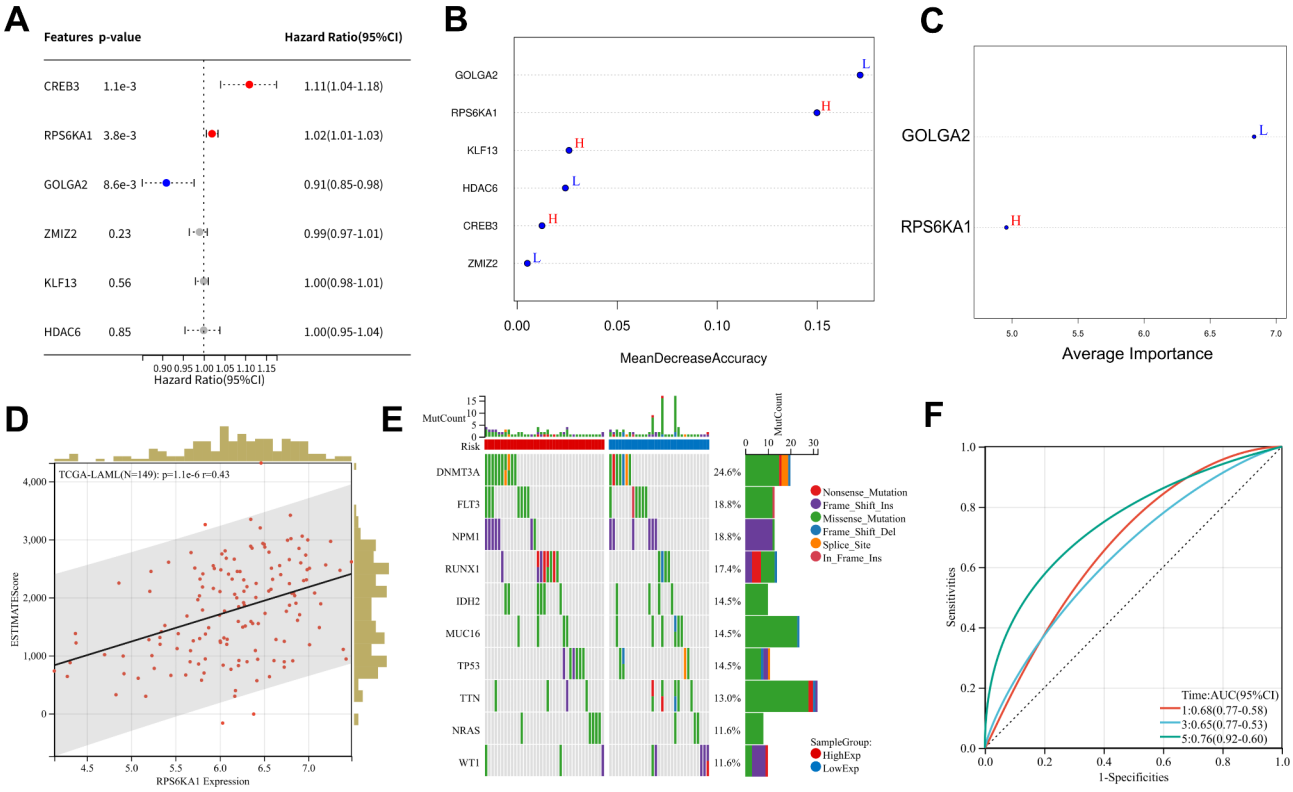

Fig. 3 Screening and analysis of key genes. **A-C**. Key genes associated with AML prognosis were identified using multivariate Cox regression analysis **(A)**, random forest **(B)**, and support vector machine **(C)** based on the six genes included in the risk model. **D**. Correlation analysis between *RPS6KA1* expression and immune infiltration score. **E**. Landscape maps with gene mutations in the samples with high and low expression of RPS6KA1. **F**. Time-dependent ROC curves were used to assess the sensitivity of *RPS6KA1* expression levels to predict the overall survival of AML patients

Knockdown of *RPS6KA1* inhibited the proliferation, migration and invasion of AML cells, and induced cell cycle arrest and apoptosis

According to the GEPIA database (http://gepia.cancer-pku.cn/), *RPS6KA1* mRNA expression in AML samples was significantly higher than in the control group (Supplementary Fig. 2A), and its high expression level was associated with shorter overall survival in AML patients (Supplementary Fig. 2B). To explore the biological role of *RPS6KA1* in AML progression, HL-60 and THP-1 cells were transfected with si-RPS6KA1 to achieve *RPS6KA1* knockdown. *RPS6KA1* depletion significantly reduced the mRNA and protein expression levels of RPS6KA1 in HL-60 and THP-1 cells (Supplementary Fig. 2C&D). Since si-RPS6KA1#1 exhibited a more pronounced knockdown efficiency, it was selected for subsequent experiments. *RPS6KA1* knockdown significantly inhibited the proliferation, migration, and invasion of HL-60 and THP-1 cells (Supplementary Fig. 2E-G). Flow cytometry analysis further revealed that *RPS6KA1* knockdown induced significant cell cycle arrest in the G0/G1 phase (Supplementary Fig. 2H&I) and increased apoptosis levels in HL-60 and THP-1 cells (Supplementary Fig. 2J&K). A recent study reported that inhibition of *RPS6KA1* enhances GSK3 activity, promotes phosphorylation of MCL-1 at serine 159 (p-MCL-1), and reduces the total expression of MCL-1, an anti-apoptotic protein, thereby contributing to AML cell resistance to venetoclax/azacitidine treatment [21]. Consistently, the present study observed a positive correlation between *RPS6KA1* expression and MCL-1 expression in AML samples from the TCGA cohort (Supplementary Fig. 2L). Furthermore, after *RPS6KA1* depletion, western blot analysis showed an increase in p-MCL-1 expression levels, while the expression levels of p-ERK1/2, p-JNK, and p-p38 were decreased (Supplementary Fig. 2M&N). Overall, these results suggest that *RPS6KA1* is highly expressed in AML and plays a role in promoting the malignant progression of the disease.

The results of molecular docking

From the HERB database (http://herb.ac.cn/), withaferin A, (-)-epigallocatechin gallate, flavopiridol, afzelin, quercetin, phorbol 12,13-dibutyrate, and resveratrol were identified as potential compounds targeting RPS6KA1 (Supplementary Table 3). To verify the interaction between RPS6KA1 and these compounds, molecular docking was performed. The results showed that afzelin binds to the RPS6KA1 protein by forming two hydrogen bonds with the LEU-144 and ASP-148 amino acid

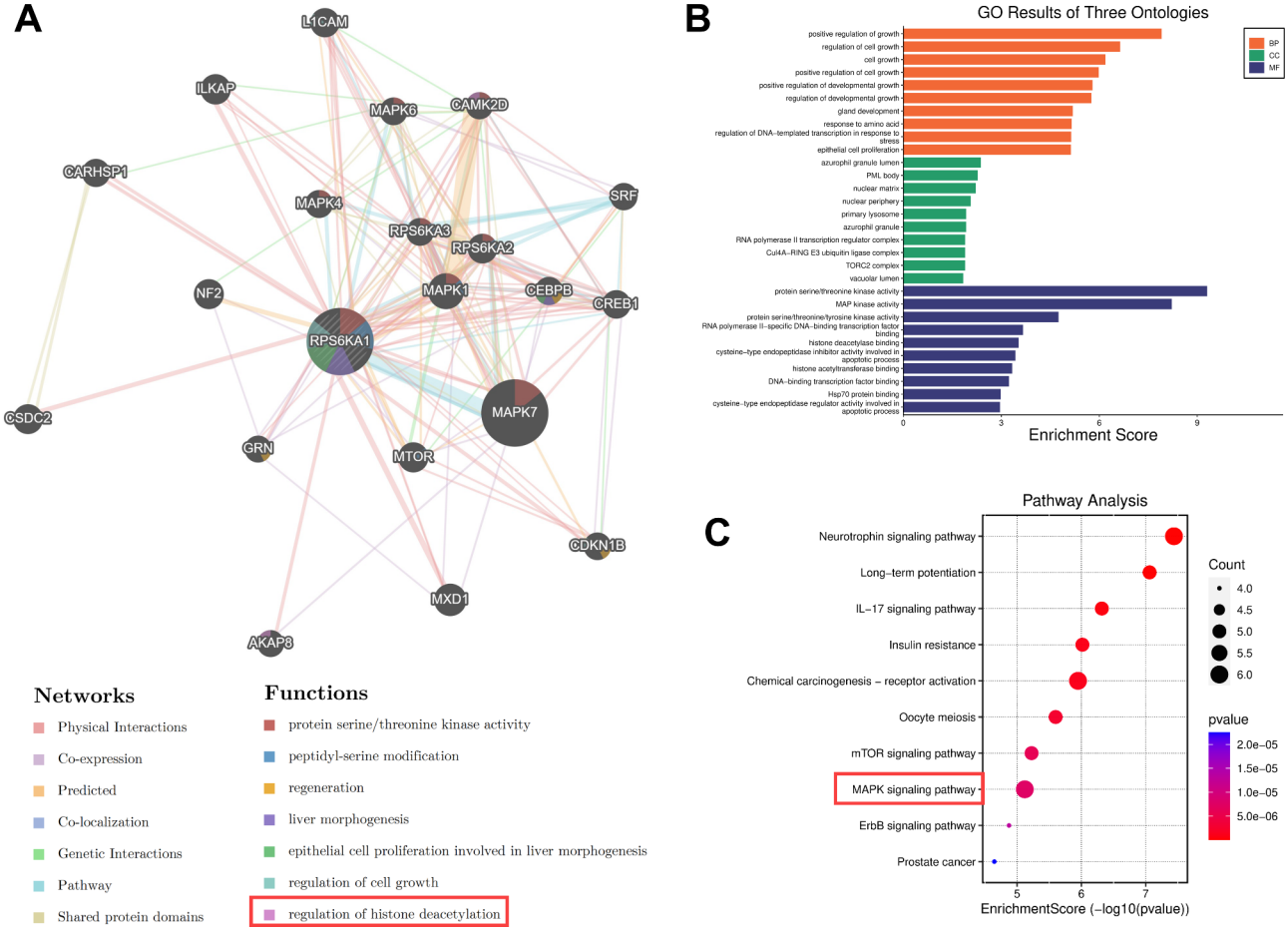

Fig. 4 Construction and analysis of gene-gene interaction network of *RPS6KA1*.**A**. The co-expression network of *RPS6KA1* gene was established by GeneMANIA. **B**. GO enrichment bar chart of *RPS6KA1* and its co-expressed genes. The horizontal axis is the enrichment score, and the vertical axis represents the biological process (yellow), cell component (green), and molecular function (dark blue). **C**. Enrichment bubble map of KEGG pathway of *RPS6KA1* and its co-expressed genes. The horizontal axis is the enrichment score, the vertical axis is the item name, the bubble color represents the *P*-value size, and the bubble size represents the gene count

residues, with a binding energy of −8.9 kcal/mol (Fig. 5A). (-)-Epigallocatechin gallate binds to RPS6KA1 by forming four hydrogen bonds with the SER-72, THR-204, GLY-147, and LYS-94 residues, with a binding energy of −8.7 kcal/mol (Fig. 5B). Flavopiridol binds to RPS6KA1 by forming two hydrogen bonds with the LEU-144 and ASP-148 residues, with a binding energy of −9.4 kcal/mol (Fig. 5C). Phorbol 12,13-dibutyrate binds to RPS6KA1 by forming two hydrogen bonds with the ASN-193 residue, with a binding energy of −8.0 kcal/mol (Fig. 5D). Quercetin binds to RPS6KA1 by forming three hydrogen bonds with the LEU-144, ASN-192, and GLU-191 residues, with a binding energy of −8.6 kcal/mol (Fig. 5E). Resveratrol binds to RPS6KA1 by forming three hydrogen bonds with the GLN-70, SER-72, and LEU-144 residues, with a binding energy of −7.2 kcal/mol (Fig. 5F). Withaferin A binds to RPS6KA1 by forming a hydrogen bond with the THR-204 residue, with a binding energy of −8.7 kcal/mol (Fig. 5G). These results indicate that RPS6KA1 has a high binding affinity with these active compounds. In this study, afzelin was chosen for further investigation.

Afzelin inhibited AML progression through repressing the activation of the MAPK pathway and RPS6KA1

To investigate the potential function and mechanism of afzelin in AML treatment, HL-60 and THP-1 cells were treated with different concentrations of afzelin (0, 10, 20, 30, 40, and 50 μM) for 24 h, and cell viability was assessed using the CCK-8 assay. The chemical structure of afzelin is shown in Fig. 6A. The results demonstrated that afzelin inhibited the viability of HL-60 and THP-1 cells in a concentration-dependent manner (Fig. 6B). The half-maximal inhibitory concentration (IC_{50}) of afzelin for HL-60 and THP-1 cells was 28.93 μM and 28.70 μM, respectively. Transwell assays revealed that afzelin treatment significantly reduced the migration and invasion capacities of HL-60 and THP-1 cells (Fig. 6C&D). Additionally, afzelin induced cell cycle arrest (Fig. 6E&F) and

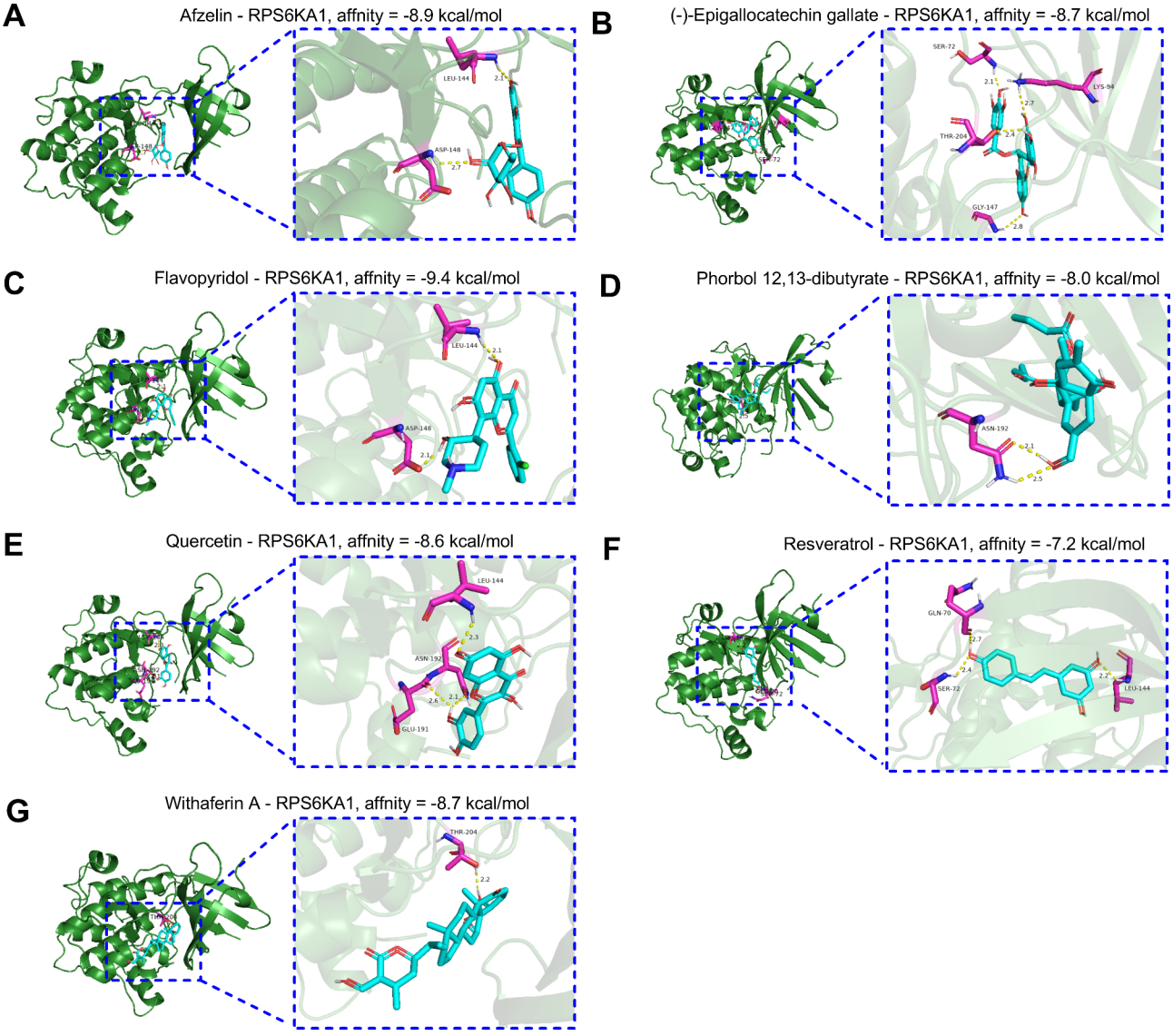

Fig. 5 The binding affinity between RPS6KA1 and drugs. Molecular docking of RPS6KA1 (PDB ID: 2Z7S) with afzelin **(A)**, (-)-epigallocatechin gallate **(B)**, flavopiridol **(C)**, phorbol 12,13-dibutyrate **(D)**, quercetin **(E)**, resveratrol **(F)**, and withaferin A **(G)**. Green represents RPS6KA1, purple represents the surrounding amino acid residues in the binding pocket, light blue represents the compound, and yellow dashed lines represent hydrogen bonds

apoptosis in both HL-60 and THP-1 cells (Fig. 6G&H). Western blot analysis showed that afzelin reduced the protein levels of p-RPS6KA1, p-ERK1/2, p-JNK, and p-p38, while increasing the level of p-MCL-1 in HL-60 and THP-1 cells (Fig. 6I&J). In this study, we also investigated the effects of afzelin on the sensitivity of AML cells to venetoclax and azacitidine. As expected, afzelin treatment markedly enhanced the inhibitory effects of venetoclax and azacitidine on the viability of HL-60 and THP-1 cells (Supplementary Fig. 3). These findings suggest that afzelin may exert anti-tumor effects in AML by repressing the MAPK pathway and inactivating RPS6KA1.

Discussion

AML is a heterogeneous disease characterized by genetic and epigenetic aberrations [22, 23]. Emerging evidence suggests that abnormal histone acetylation is closely associated with the onset and progression of AML [14]. Dysregulation of HDACs has been identified as a key factor in AML, contributing to poorer prognosis [24]. Furthermore, risk models based on histone acetylation regulators have demonstrated significant predictive value in assessing the prognosis of patients with breast cancer and renal clear cell carcinoma [25–27].

In this study, we constructed a gene-gene interaction network based on 36 known histone acetylation regulators and identified 301 histone acetylation-related genes

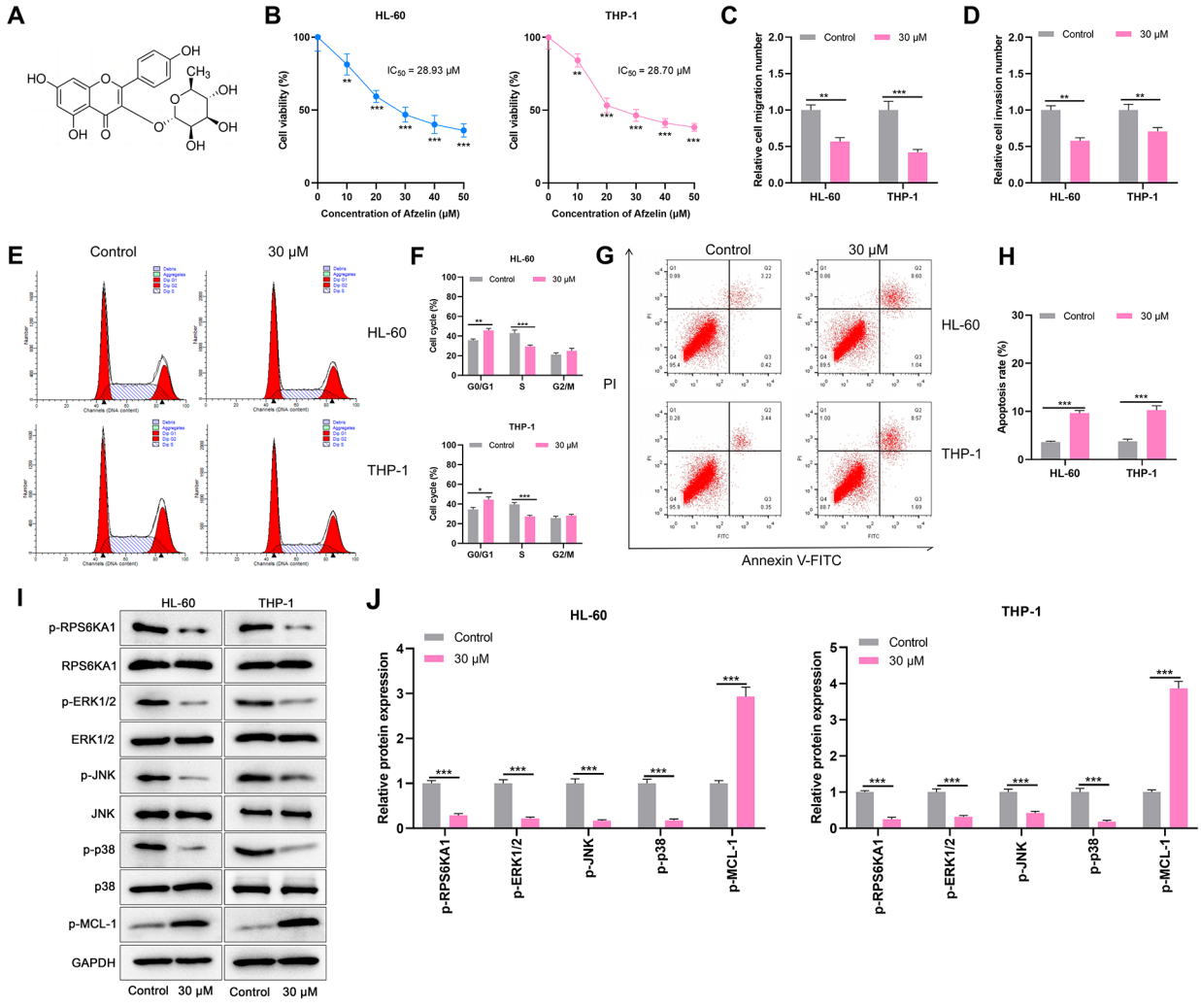

Fig. 6 Afzelin exerts anti-AML effects by acting on the MAPK pathway and RPS6KA1. **A**. Chemical structure of afzelin. **B**. HL-60 and THP-1 cells were treated with different concentrations of afzelin (0, 10, 20, 30, 40 and 50 μM) for 24 h, and cell viability was detected by the CCK-8 assay. **C-H**. The migration (C), invasion (D), cell cycle (E&F), and apoptosis (G&H) of HL-60 and THP-1 cells after treatment with 30 μM afzelin for 24 h were detected by Transwell assay and flow cytometry, respectively. **I&J**. Protein levels of p-RPS6KA1, p-ERK1/2, p-JNK, p-p38, and p-MCL-1 in HL-60 and THP-1 cells treated with 30 μM afzelin for 24 h were detected by Western blot. *$P < 0.05$, **$P < 0.01$, ***$P < 0.001$

through correlation analysis. From these, six key genes, including *CREB3*, *KLF13*, *RPS6KA1*, *ZMIZ2*, *HDAC6*, and *GOLGA2*, were selected to develop a risk model for predicting the prognosis of AML and calculating the risk score. This risk model was shown to be an independent risk factor for poor prognosis in AML patients. Immune regulation plays a crucial role in the tumorigenesis and progression of AML, with immune infiltration levels being a key factor in determining the response to immunotherapy and patient prognosis [28, 29]. In this study, significant differences were observed in 9 out of 22 immune cell types between the high-risk and low-risk groups. The high-risk group exhibited a higher proportion of monocytes and activated memory $CD4^+$ T cells. Additionally, we found a negative correlation between the risk score and the level of immune infiltration. These findings suggest that the poor prognosis observed in high-risk AML patients may be linked to immunosuppression within the tumor microenvironment, and that targeting abnormal histone acetylation could enhance the efficacy of immunotherapy in AML treatment.

In this study, *RPS6KA1* was identified as a key independent risk factor for predicting the prognosis of AML patients and was found to be associated with immune infiltration levels. RPS6KA1, also known as ribosomal S6 kinase 1 (RSK1), is a member of the ribosomal S6 kinase protein family [30]. It is located in the cytoplasm and acts as a downstream effector of the Ras/Raf/MAPK signaling pathway, regulating cell proliferation, survival, and migration through the phosphorylation of various substrates

[31–33]. *RPS6KA1* has been reported to be highly expressed in prostate carcinoma, breast carcinoma, and nodular melanoma, where its hyperactivation promotes tumor growth and invasion and is associated with poor prognosis [30, 34, 35]. Notably, recent studies have also reported that *RPS6KA1* is linked to poor prognosis and chemotherapy resistance in AML patients [21, 36]. Consistently, our study demonstrated that *RPS6KA1* was highly expressed in AML and that its high expression was predictive of a worse prognosis. Bioinformatics analysis suggested that its abnormal expression is linked to the MAPK, IL-17, mTOR, and ErbB signaling pathways, which are crucial modulators in human malignancies. Additionally, *RPS6KA1* knockdown inhibited the proliferation, migration, and invasion of AML cells, while inducing cell cycle arrest and apoptosis. Collectively, these findings validate RPS6KA1 as an oncoprotein in AML. However, it should be noted that, although our data indicate a correlation between *RPS6KA1* and histone deacetylation status in AML, the precise mechanisms by which *RPS6KA1* modulates histone deacetylation regulators, or how histone deacetylation affects *RPS6KA1* expression, remain unclear. These mechanisms warrant further exploration in future studies.

Molecular docking showed that afzelin, (-)-epigallocatechin gallate, flavopiridol, phorbol 12,13-dibutyrate, quercetin, resveratrol, and withaferin A all exhibited good binding affinity with RPS6KA1. Previous studies have confirmed that (-)-epigallocatechin gallate, flavopiridol, phorbol 12,13-dibutyrate, quercetin, resveratrol, and withaferin A have significant anti-AML activities [37–42]. However, the tumor-suppressive effect of afzelin on AML cells has not been previously clarified. Afzelin, also known as kaempferol-3-o-rhamnoside, is a flavonol glycoside commonly used in the preparation of antibacterial and anti-inflammatory agents. It is readily available as it is found in various plants, including houttuynia, pepper, dried ginger, water lilies, and ginkgo biloba [43, 44]. Afzelin has been reported to inhibit the migration of triple-negative breast carcinoma cells by targeting ERK2/MAPK1, KRas, and FAK [45]. It also inhibit the proliferation of lung, gastric, and prostate carcinoma cells [46–48]. Notably, this study found that afzelin could inhibit the viability, migration, and invasion of AML cells, as well as induce cell cycle arrest and apoptosis. Mechanistically, afzelin treatment reduced the protein levels of p-RPS6KA1, p-ERK1/2, p-JNK, and p-p38 in AML cells while promoting the level of p-MCL-1, suggesting that afzelin inhibits RPS6KA1 activation both by directly binding to it and by repressing its upstream MAPK signaling. Previous studies have suggested that *RPS6KA1* contributes to AML progression and drug resistance by promoting MCL-1 expression [21, 49], implying that afzelin treatment may sensitize AML cells to chemotherapeutics such as venetoclax and azacitidine. As expected, in this study, in vitro assays demonstrated that afzelin synergistically suppressed the viability of AML cells when combined with venetoclax or azacitidine. These results suggest that afzelin is a promising natural compound for overcoming chemoresistance in AML cells.

Conclusions

This study successfully constructs a novel risk model associated with histone acetylation for AML, offering a promising tool for predicting the prognosis of AML patients. Additionally, we validate RPS6KA1 as an oncoprotein in AML, and identify afzelin as a potential anti-AML agent. Moving forward, the reliability of these findings, particularly the biological function and pharmacological effects of *RPS6KA1* and afzelin, should be confirmed through in vivo experiments and clinical trials. Furthermore, a larger cohort is needed to verify the accuracy and validity of the risk model.

Abbreviations

AML	acute myeloid leukemia
OS	overall survival
HATs	histone acetyltransferases
HDACs	histone deacetylases
RPS6KA1	ribosomal protein S6 kinase A1
TCGA	the Cancer Genome Atlas
FPKM	fragments per kilobase of exon model per million mapped
GEO	Gene Expression Omnibus
LASSO	least absolute shrinkage and selection operator
ROC	receiver operating characteristic
AUC	area under the curve
PCA	principal component analysis
HR	hazard ratio
DEGs	differentially expressed genes
KEGG	Kyoto Encyclopedia of Genes and Genomes
ESTIMATE	Estimation of Stromal and Immune Cells in Malignant Tumors using the Expression Data
GO	gene ontology
PDB	Protein Data Bank
DMEM	Dulbecco's Modified Eagle's Medium
FBS	fetal bovine serum
siRNA	small interfering RNA
si-NC	siRNA negative controls
qPCR	Quantitative real-time PCR
CCK-8	cell counting kit-8
OD	optical density
PI	propyl iodide
FITC	Fluorescein Isothiocyanate
PVDF	polyvinylidene fluoride
SD	standard deviation
RSK1	ribosomal S6 kinase 1
MCL-1	MCL1 apoptosis regulator, BCL2 family member

Supplementary Information

The online version contains supplementary material available at https://doi.org/10.1186/s12885-024-12886-3.

Supplementary Material 1

Supplementary Material 2

Acknowledgements
We thank Language Science (http://www.lansci.com.cn/) for the language editing service.

Author contributions
Conceived and designed the experiments: Ziwen Guo and Yongbin Ye; Performed the experiments: Xiaojuan Guo, Guinian Huang and Dafa Qiu; Analyzed the data: Huiqing He1 and Xiaomin Niu; Wrote the paper: Xiaojuan Guo and Guinian Huang.All authors read and approved the final manuscript.

Funding
This study was supported by Zhongshan Science and Technology Research Major Project (No. 2021B3010) and Zhongshan Science and Technology Research Project (No.2022B1135).

Data availability
The data used to support the findings of this study are available from the corresponding author upon request.

Declarations

Ethics approval and consent to participate
Not applicable.

Consent for publication
Not applicable.

Competing interests
The authors declare no competing interests.

Received: 24 January 2024 / Accepted: 2 September 2024
Published online: 27 September 2024

References

1. Miljkovic-Licina M, Arraud N, Zahra AD, Ropraz P, Matthes T. Quantification and phenotypic characterization of Extracellular vesicles from patients with Acute Myeloid and B-Cell Lymphoblastic Leukemia. Cancers (Basel). 2021;14(1):56.
2. Hernandez-Valladares M, Wangen R, Aasebø E, Reikvam H, Berven FS, Selheim F, Bruserud Ø. Proteomic studies of primary Acute myeloid leukemia cells derived from patients before and during disease-stabilizing treatment based on all-Trans Retinoic Acid and Valproic Acid. Cancers (Basel). 2021;13(9):2143.
3. San José-Enériz E, Gimenez-Camino N, Agirre X, Prosper F. HDAC inhibitors in Acute myeloid leukemia. Cancers (Basel). 2019;11(11):1794.
4. Siegel RL, Miller KD, Fuchs HE, Jemal A. Cancer statistics, 2021. CA Cancer J Clin. 2021;71(1):7–33.
5. Liu W, Wu Z, Yu Y, Qiao C, Zhu H, Hong M, Zhu Y, Qian S, Chen S, Wu D, Li J, Jin H. Functional evaluation of KEL as an oncogenic gene in the progression of Acute Erythroleukemia. Oxid Med Cell Longev. 2022;2022:5885342.
6. Lee JB, Vasic D, Kang H, Fang KK, Zhang L. State-of-art of Cellular Therapy for Acute Leukemia. Int J Mol Sci. 2021;22(9):4590.
7. Lee JE, Kwon CS, Jeon BE, Kim WR, Lee DH, Koh S, Kim HS, Kim SW. Genome-wide gene expression profiling defines the mechanism of Anticancer Effect of Colorectal Cancer Cell-Derived Conditioned Medium on Acute myeloid leukemia. Genes (Basel). 2022;13(5):883.
8. Cao J, Yan Q, Cancer Epigenetics. Tumor immunity, and Immunotherapy. Trends Cancer. 2020;6(7):580–92.
9. Bhat KP, Ümit Kaniskan H, Jin J, Gozani O. Epigenetics and beyond: targeting writers of protein lysine methylation to treat disease. Nat Rev Drug Discov. 2021;20(4):265–86.
10. Liu S, Chang W, Jin Y, Feng C, Wu S, He J, Xu T. The function of histone acetylation in cervical cancer development. Biosci Rep. 2019;39(4):BSR20190527.
11. Cai J, Deng Y, Min Z, Li C, Zhao Z, Jing D. Deciphering the dynamics: exploring the impact of mechanical forces on histone acetylation. FASEB J. 2024;38(15):e23849.
12. Hałasa M, Wawruszak A, Przybyszewska A, Jaruga A, Guz M, Kałafut J, Stepulak A, Cybulski M. H3K18Ac as a marker of Cancer Progression and potential target of Anti-cancer Therapy. Cells. 2019;8(5):485.
13. Chen C, Liu J. Histone acetylation modifications: a potential targets for the diagnosis and treatment of papillary thyroid cancer. Front Oncol. 2022;12:1053618.
14. Yan F, Li J, Milosevic J, Petroni R, Liu S, Shi Z, Yuan S, Reynaga JM, Qi Y, Rico J, Yu S, Liu Y, Rokudai S, Palmisiano N, Meyer SE, Sung PJ, Wan L, Lan F, Garcia BA, Stanger BZ, Sykes DB, Blanco MA. KAT6A and ENL Form an Epigenetic Transcriptional Control Module to drive critical leukemogenic gene-expression programs. Cancer Discov. 2022;12(3):792–811.
15. Pal D, Raj K, Nandi SS, Sinha S, Mishra A, Mondal A, Lagoa R, Burcher JT, Bishayee A. Potential of synthetic and natural compounds as Novel histone deacetylase inhibitors for the Treatment of Hematological Malignancies. Cancers (Basel). 2023;15(10):2808.
16. Issa GC, Aldoss I, DiPersio J, Cuglievan B, Stone R, Arellano M, Thirman MJ, Patel MR, Dickens DS, Shenoy S, Shukla N, Kantarjian H, Armstrong SA, Perner F, Perry JA, Rosen G, Bagley RG, Meyers ML, Ordentlich P, Gu Y, Kumar V, Smith S, McGeehan GM, Stein EM. The menin inhibitor revumenib in KMT2A-rearranged or NPM1-mutant leukaemia. Nature. 2023;615(7954):920–4.
17. Mehndiratta S, Liou JP. Histone lysine specific demethylase 1 inhibitors. RSC Med Chem. 2020;11(9):969–81.
18. Urwanisch L, Unger MS, Sieberer H, Dang HH, Neuper T, Regl C, Vetter J, Schaller S, Winkler SM, Kerschbamer E, Weichenberger CX, Krenn PW, Luciano M, Pleyer L, Greil R, Huber CG, Aberger F, Horejs-Hoeck J. The class IIA histone deacetylase (HDAC) inhibitor TMP269 downregulates ribosomal proteins and has anti-proliferative and pro-apoptotic effects on AML cells. Cancers (Basel). 2023;15(4):1039.
19. Long X, Liu L, Zhao Q, Xu X, Liu P, Zhang G, Lin J. Comprehensive Analysis of Tripterine Anti-ovarian Cancer effects using Weighted Gene Co-expression Network Analysis and Molecular Docking. Med Sci Monit. 2022;28:e932139.
20. Na K, Li K, Sang T, Wu K, Wang Y, Wang X. Anticarcinogenic effects of water extract of sporoderm-broken spores of Ganoderma lucidum on colorectal cancer in vitro and in vivo. Int J Oncol. 2017;50(5):1541–54.
21. Weidenauer K, Schmidt C, Rohde C, Pauli C, Blank MF, Heid D, Waclawiczek A, Corbacioglu A, Göllner S, Lotze M, Vierbaum L, Renders S, Krijgsveld J, Raffel S, Sauer T, Trumpp A, Pabst C, Müller-Tidow C, Janssen M. The ribosomal protein S6 kinase alpha-1 (RPS6KA1) induces resistance to venetoclax/azacitidine in acute myeloid leukemia. Leukemia. 2023;37(8):1611–25.
22. Chen J, Liu L, Ma R, Pang A, Yang D, Chen X, Wei J, He Y, Zhang R, Zhai W, Ma Q, Jiang E, Han M, Zhou J, Feng S. Outcome of autologous stem cell transplantation in patients with favorable-risk acute myeloid leukemia in first remission. Cancer Cell Int. 2022;22(1):332.
23. Seo W, Silwal P, Song IC, Jo EK. The dual role of autophagy in acute myeloid leukemia. J Hematol Oncol. 2022;15(1):51.
24. Yao J, Li G, Cui Z, Chen P, Wang J, Hu Z, Zhang L, Wei L. The histone deacetylase inhibitor I1 induces differentiation of Acute Leukemia cells with MLL gene rearrangements via epigenetic modification. Front Pharmacol. 2022;13:876076.
25. Dai Q, Ye Y. Development and validation of a Novel histone acetylation-related gene signature for Predicting the Prognosis of Ovarian Cancer. Front Cell Dev Biol. 2022;10:793425.
26. Wang S, Xiang T, Yu L, Wen J, Liu F, Yang D, Wu W, Hu L. Novel molecular subtypes and related score based on histone acetylation modification in Renal Clear Cell Carcinoma. Front Cell Dev Biol. 2021;9:668810.
27. Wang W, Shen Y, Zhang P, Liu L, Sha X, Li H, Wang S, Zhang H, Zhou Y, Shi J. Histone acetylation modification regulator-mediated tumor microenvironment infiltration characteristics and prognostic model of lung adenocarcinoma patients. J Thorac Dis. 2022;14(10):3886–902.
28. Tu J, Wang D, Zheng X, Liu B. Single-cell RNA datasets and bulk RNA datasets analysis demonstrated C1Q + tumor-associated macrophage as a major and antitumor immune cell population in osteosarcoma. Front Immunol. 2023;14:911368.
29. Guo G, Li B, Li Q, Li C, Guo D. PTPRC overexpression predicts poor prognosis and correlates with Immune Cell Infiltration in Pediatric Acute myeloid leukemia. Clin Lab. 2022;68(7).
30. Czaplinska D, Gorska M, Mieczkowski K, Peszynska-Sularz G, Zaczek AJ, Romanska HM, Sadej R. RSK1 promotes murine breast cancer growth and metastasis. Folia Histochem Cytobiol. 2018;56(1):11–20.
31. Shareefi G, Turkistani AN, Alsayyah A, Kussaibi H, Abdel Hadi M, Alkharsah KR. Pathway-affecting single nucleotide polymorphisms (SNPs) in RPS6KA1 and MBIP genes are Associated with breast Cancer risk. Asian Pac J Cancer Prev. 2020;21(7):2163–8.
32. Anjum R, Blenis J. The RSK family of kinases: emerging roles in cellular signalling. Nat Rev Mol Cell Biol. 2008;9(10):747–58.

33. Wong TY, Menaga S, Huang CF, Ho SHA, Gan SC, Lim YM. 2-Methoxy-1,4-naphthoquinone (MNQ) regulates cancer key genes of MAPK, PI3K, and NF-κB pathways in Raji cells. Genomics Inf. 2022;20(1):e7.
34. Clark DE, Errington TM, Smith JA, Frierson HF Jr, Weber MJ, Lannigan DA. The serine/threonine protein kinase, p90 ribosomal S6 kinase, is an important regulator of prostate cancer cell proliferation. Cancer Res. 2005;65(8):3108–16.
35. Salhi A, Farhadian JA, Giles KM, Vega-Saenz de Miera E, Silva IP, Bourque C, Yeh K, Chhangawala S, Wang J, Ye F, Zhang DY, Hernando-Monge E, Houvras Y, Osman I. RSK1 activation promotes invasion in nodular melanoma. Am J Pathol. 2015;185(3):704–16.
36. Yu DH, Chen C, Liu XP, Yao J, Li S, Ruan XL. Dysregulation of miR-138-5p/RPS6KA1-AP2M1 is Associated with Poor Prognosis in AML. Front Cell Dev Biol. 2021;9:641629.
37. Della Via FI, Shiraishi RN, Santos I, Ferro KP, Salazar-Terreros MJ, Franchi Junior GC, Rego EM, Saad STO, Torello CO. (-)-Epigallocatechin-3-gallate induces apoptosis and differentiation in leukaemia by targeting reactive oxygen species and PIN1. Sci Rep. 2021;11(1):9103.
38. Chen KTJ, Militao GGC, Anantha M, Witzigmann D, Leung AWY, Bally MB. Development and characterization of a novel flavopiridol formulation for treatment of acute myeloid leukemia. J Control Release. 2021;333:246–57.
39. Gobbi G, Mirandola P, Carubbi C, Micheloni C, Malinverno C, Lunghi P, Bonati A, Vitale M. Phorbol ester-induced PKCepsilon down-modulation sensitizes AML cells to TRAIL-induced apoptosis and cell differentiation. Blood. 2009;113(13):3080–7.
40. Xiao J, Zhang B, Yin S, Xie S, Huang K, Wang J, Yang W, Liu H, Zhang G, Liu X, Li Y, Nie D. Quercetin induces autophagy-associated death in HL-60 cells through CaMKKβ/AMPK/mTOR signal pathway. Acta Biochim Biophys Sin (Shanghai). 2022;54(9):1244–56.
41. Ersöz NŞ, Adan A. Resveratrol triggers anti-proliferative and apoptotic effects in FLT3-ITD-positive acute myeloid leukemia cells via inhibiting ceramide catabolism enzymes. Med Oncol. 2022;39(3):35.
42. Clesham K, Walf-Vorderwülbecke V, Gasparoli L, Virely C, Cantilena S, Tsakaneli A, Inglott S, Adams S, Samarasinghe S, Bartram J, Williams G, de Boer J, Williams O. Identification of a c-MYB-directed therapeutic for acute myeloid leukemia. Leukemia. 2022;36(6):1541–9.
43. Sun Y, Guo D, Yue S, Zhou M, Wang D, Chen F, Wang L. Afzelin protects against doxorubicin-induced cardiotoxicity by promoting the AMPKα/SIRT1 signaling pathway. Toxicol Appl Pharmacol. 2023;477:116687.
44. Afendi FM, Okada T, Yamazaki M, Hirai-Morita A, Nakamura Y, Nakamura K, Ikeda S, Takahashi H, Altaf-Ul-Amin M, Darusman LK, Saito K, Kanaya S. KNApSAcK family databases: integrated metabolite-plant species databases for multifaceted plant research. Plant Cell Physiol. 2012;53(2):e1.
45. Rachmi E, Purnomo BB, Endharti AT, Fitri LE. Identification of afzelin potential targets in inhibiting triple-negative breast cancer cell migration using reverse docking. Porto Biomed J. 2020;5(6):e095.
46. Xia L, Xu X, Li M, Zhang X, Cao F. Afzelin induces immunogenic cell death against lung cancer by targeting NQO2. BMC Complement Med Ther. 2023;23(1):381.
47. Radziejewska I, Supruniuk K, Czarnomysy R, Buzun K, Bielawska A. Anti-cancer potential of Afzelin towards AGS gastric Cancer cells. Pharmaceuticals (Basel). 2021;14(10):973.
48. Zhu KC, Sun JM, Shen JG, Jin JZ, Liu F, Xu XL, Chen L, Liu LT, Lv JJ. Afzelin exhibits anti-cancer activity against androgen-sensitive LNCaP and androgen-independent PC-3 prostate cancer cells through the inhibition of LIM domain kinase 1. Oncol Lett. 2015;10(4):2359–65.
49. Zhang Q, Riley-Gillis B, Han L, Jia Y, Lodi A, Zhang H, Ganesan S, Pan R, Konoplev SN, Sweeney SR, Ryan JA, Jitkova Y, Dunner K Jr, Grosskurth SE, Vijay P, Ghosh S, Lu C, Ma W, Kurtz S, Ruvolo VR, Ma H, Weng CC, Ramage CL, Baran N, Shi C, Cai T, Davis RE, Battula VL, Mi Y, Wang J, DiNardo CD, Andreeff M, Tyner JW, Schimmer A, Letai A, Padua RA, Bueso-Ramos CE, Tiziani S, Leverson J, Popovic R, Konopleva M. Activation of RAS/MAPK pathway confers MCL-1 mediated acquired resistance to BCL-2 inhibitor venetoclax in acute myeloid leukemia. Signal Transduct Target Ther. 2022;7(1):51.

Publisher's note